Asymmetry of Frequency Distribution in Power Systems: Sources, Estimation, Impact and Control

Taulant Kërçi, *IEEE Senior Member,* and Federico Milano, *IEEE Fellow*

***Abstract*—This paper analyses an emerging real-world phenomena in inverter-based renewable-dominated power systems, namely, asymmetry of frequency distribution. The paper first provides a rationale on why asymmetry reduces the "quality" of the frequency control and system operation. Then it provides qualitative theoretical insights that explain asymmetry in terms of the nonlinearity of real-world power systems and associated models. In particular network losses and pitch angle-based frequency control of wind power plants are discussed. Then the paper proposes a nonlinear compensation control to reduce the asymmetry as well as a statistical metric based on the frequency probability distribution to quantify the level of asymmetry in a power system. Real-world data obtained from the Irish and Australian transmission systems serve to support the theoretical appraisal, whereas simulations based on an IEEE benchmark system show the effectiveness of the proposed nonlinear compensation. The case study also shows that, while automatic generation control reduces asymmetry, frequency control limits and droop-based frequency support provided by wind generation using a tight deadband of $\pm$15 mHz, namely active power control, leads to a significant increase in the asymmetry of the frequency probability distribution.**

***Index Terms*—Frequency quality, primary frequency control (PFC), active power control (APC), automatic generation control (AGC), frequency probability distribution (FPD).**

I. Introduction

A. Motivation

INTUITIVELY, the higher the symmetry in the dynamic response of a dynamical system, the higher the predictability of the system behavior and controllability. Thus, a precise evaluation of the asymmetries present in a system contributes towards increased power system stability and resilience. The equations that represent power systems are for the most part symmetrical. However, it has been recently observed by some transmission system operators (TSOs), that power systems are becoming increasingly (and unexpectedly) asymmetrical [1], [2]. In this context, the aim of this paper is to study the causes of frequency probability distribution (FPD) asymmetry in power systems, provide a qualitative theoretical appraisal of this asymmetry; and, finally, show how asymmetry can be compensated through modified control.

B. Literature Review

The topic of FPD in power systems and the various sources and parameters that influence it has recently received attention in the literature, in particular, in light of the integration of uncertain and variable renewable energy sources (RESs) such as wind and solar generation [3]–[8]. The main focus of these works is on the modelling and study of how to reproduce the frequency distribution observed in real grids, e.g., the bi-modal distribution. However, the effect of losses, control limits and RESs providing primary frequency control (PFC) has not been considered so far.

With regard to the latter, there is a concern in the industry that enforcing RESs such as wind and solar generation providing PFC with narrow deadband (e.g., $\pm$15 mHz) is contributing to new phenomena arising in power systems (so far unexplained) such as low-frequency oscillations and asymmetry in the frequency distribution [2]. Specifically, the Australian Energy Market Operator (AEMO) has recently acknowledged feedback from industry that: "*the universal application of very narrow governor deadbands may be contributing to unexplained oscillations from some plant and asymmetry in the NEM's frequency characteristic.*", and considers this an issue worth exploring further [2]. In addition, the Australian Energy Council (AEC) and, in general, power system industry in Australia, is concerned that this asymmetry is decreasing power system resilience as reported in [1]: "*Furthermore, since the introduction of mandatory PFR, power system frequency has been exhibiting behaviour that suggests resilience has decreased. As confirmed in the report prepared by Provecta commissioned by the Australian Energy Council (AEC) as part of its submission to the Draft Determination, system-wide frequency is displaying:*

- *A "wobble" in terms of a slow frequency cycling with a period 18-24 seconds.*
- *A "skew" in terms of an asymmetry in the distribution.*

Thus, it is difficult to see how any contribution to improved power system resilience is realised particularly in view of the above comments."

These excerpts indicate that the changing dynamic behavior of power systems (which can manifest as the appearance of new phenomena such as asymmetry of the FPD) is yet to be fully understood [9]. Among the few recent works that have studied the issue of asymmetry of FPD in power systems, for example, we cite [10], [11]. Both works utilize the skewness parameter β_f to measure asymmetry of the distribution. However, these works aim at identifying the issue rather than fully explain its causes. Moreover, these works do not propose ways to compensate the asymmetry. This paper aims at filling these gaps.

T. Kërçi is with EirGrid plc, Transmission System Operator, Dublin, D04 FW28, Ireland. F. Milano is with School of Electrical and Electronic Engineering, University College Dublin, Dublin, D04V1W8, Ireland. E-mails: taulant.kerci@eirgrid.com, federico.milano@ucd.ie.

This work was partially supported by Science Foundation Ireland (SFI) by funding F. Milano under NexSys project, Grant No. 21/SPP/3756.

C. Contributions

This work contributes towards the understanding of the causes of the asymmetry of FPD and proposes how to measure and compensate it. Specific novel contributions are as follows.

- Provide analytical insights into the nonlinear relationship between wind speed of wind turbines and system losses and frequency deviation.
- Propose a metric to quantify the level of asymmetry in power systems. This metric is the difference between left and right standard deviations of the FPD. It allows evaluating the "quality" of frequency control of different power systems without the need of complex techniques/methods (i.e., only frequency measurements are required that are widely available).
- Study the sources of asymmetry in power systems, such as losses, control limits, and wind generation providing PFC and Active Power Control (APC). The latter is a PFC with a tight ($\pm$ 15 mHz) deadband [12].
- Show that Automatic Generation Control (AGC) is beneficial to reduce FPD asymmetry.
- Propose a new nonlinear compensation for PFC and show its effectiveness to reduce the FPD asymmetry.
- Show through real-world data obtained from the Irish and Australian transmission grids and dynamic stochastic simulations that RESs (in particular, wind generation) are a source of asymmetry.

D. Organization

The remainder of the paper is organized as follows. Section II provides a qualitative appraisal of the causes of the asymmetry in the frequency distribution of power systems and presents the proposed control strategy to compensate this asymmetry. Section III defines various metrics, including the one proposed in this paper, to evaluate the asymmetry of the frequency distribution. Section IV illustrates two real-world examples, namely the Irish and Australian transmission systems, where the FPD asymmetry has been observed as a direct consequence of the high penetration of wind power generation. Section V describes several scenarios based on the WSCC 9-bus system benchmark system and illustrates the proposed metrics and compensation control. Finally, Section VI draws conclusions and outlines future work.

II. Qualitative Appraisal of Asymmetry

In this section, we show that the cause of the skewness of the distribution of the states of a power system is due to the nonlinearity of the equations of the system itself (Section II-A). Then, we discuss two specific examples of nonlinearity that lead to the asymmetry of the FPD, namely network losses (Section II-B) and wind frequency control obtained with variable pitch angle blades (Section II-C). We also briefly discuss the effect of regulator hard limits (Section II-D) as well as introduces the proposed control-based nonlinear compensation to reduce FPD asymmetry (Section II-E).

A. Probability Distribution of System Variables

The power system model considered in this work is the following set of Stochastic Differential Algebraic Equations (SDAEs) [13]:

$$\dot{\boldsymbol{x}} = \boldsymbol{f}(\boldsymbol{x}, \boldsymbol{y}, \boldsymbol{\eta}) \,, \tag{1}$$

$$\mathbf{0}_m = \boldsymbol{g}(\boldsymbol{x}, \boldsymbol{y}, \boldsymbol{\eta}) \,, \tag{2}$$

$$\dot{\boldsymbol{\eta}} = \boldsymbol{a}(\boldsymbol{\eta}) + \mathcal{B}(\boldsymbol{\eta})\, \boldsymbol{\xi} \,. \tag{3}$$

The transient behavior of electric power systems is traditionally described through the set of DAEs in (1)-(2). $\boldsymbol{f}$ ($\boldsymbol{f} : \mathbb{R}^{n+m+p} \mapsto \mathbb{R}^n$) are deterministic differential equations; $\boldsymbol{g}$ ($\boldsymbol{g} : \mathbb{R}^{n+m+p} \mapsto \mathbb{R}^m$) are the algebraic equations; $\boldsymbol{x}$ ($\boldsymbol{x} \in \mathbb{R}^n$) are the deterministic state variables and $\boldsymbol{y}$ ($\boldsymbol{y} \in \mathbb{R}^m$) are the algebraic variables. The stochastic processes $\boldsymbol{\eta}$ ($\boldsymbol{\eta} \in \mathbb{R}^p$) are expressed as set of stochastic differential equations, where $\boldsymbol{\xi}$ ($\boldsymbol{\xi} \in \mathbb{R}^q$) is the vector of white noise processes that represent the time derivatives of the Wiener processes. The stochastic processes are defined by a drift $\boldsymbol{a}$ ($\boldsymbol{a} : \mathbb{R}^{n+m+p} \mapsto \mathbb{R}^p$) and a diffusion term $\mathcal{B}$, where $\mathcal{B}$ is a $p \times q$ matrix. In the remainder of this work (except for the last scenario of the case study), we assume that $\boldsymbol{\eta}$ are normally distributed and represent variations of load power consumption or of the wind speed.

It is possible to show that if the system is linear and $\boldsymbol{\eta}$ are normally distributed, then also $\boldsymbol{x}$ and $\boldsymbol{y}$ are normally distributed. In fact, a linear system is written as:

$$\begin{aligned} \dot{\boldsymbol{x}} &= \mathbf{F}_{xx}\boldsymbol{x} + \mathbf{F}_{xy}\boldsymbol{y} + \mathbf{F}_{x\eta}\boldsymbol{\eta} \,, \\ \mathbf{0}_m &= \mathbf{G}_{yx}\boldsymbol{x} + \mathbf{G}_{yy}\boldsymbol{y} + \mathbf{G}_{y\eta}\boldsymbol{\eta} \,, \\ \dot{\boldsymbol{\eta}} &= \mathbf{A}_{\eta\eta}\boldsymbol{\eta} + \mathbf{B}_{\eta\xi}\,\boldsymbol{\xi} \,, \end{aligned} \tag{4}$$

where all matrices are time-invariant. This system can be rewritten as:

$$\begin{aligned} \begin{bmatrix} \dot{\boldsymbol{x}} \\ \dot{\boldsymbol{\eta}} \end{bmatrix} &= \begin{bmatrix} \mathbf{F}_{xx} - \mathbf{F}_{xy}\mathbf{E} & \mathbf{F}_{x\eta} - \mathbf{F}_{xy}\mathbf{E} \\ \mathbf{0}_{p,n} & \boldsymbol{A}_{\eta\eta} \end{bmatrix} \begin{bmatrix} \boldsymbol{x} \\ \boldsymbol{\eta} \end{bmatrix} + \begin{bmatrix} \mathbf{0}_{n,q} \\ \mathbf{B}_{\eta\xi} \end{bmatrix} \boldsymbol{\xi} \\ &= \mathbf{A}\,\boldsymbol{z} + \mathbf{B}\,\boldsymbol{\xi} \,, \end{aligned} \tag{5}$$

where $\mathbf{E} = \mathbf{G}_{yy}^{-1}\mathbf{G}_{yx}$ and $\boldsymbol{z} = [\boldsymbol{x}^T, \boldsymbol{\eta}^T]^T$ and the algebraic variables $\boldsymbol{y}$ have been eliminated using the expression:

$$\boldsymbol{y} = -\begin{bmatrix} \mathbf{G}_{yy}^{-1}\mathbf{G}_{yx} & \mathbf{G}_{yy}^{-1}\mathbf{G}_{y\eta} \end{bmatrix} \boldsymbol{z} \,. \tag{6}$$

Then, the Fokker-Planck equation allows writing the following probability distribution of all state variables in stationary condition [14]:

$$\mathbf{P}(\boldsymbol{z}) = (\det \mid 2\pi\mathbf{C} \mid)^{-1/2} \cdot \exp\!\left(-\frac{1}{2}\boldsymbol{z}^T\mathbf{C}^{-1}\boldsymbol{z} \right), \tag{7}$$

where $\mathbf{C}$ is the co-variance matrix of the state variables in (5) obtained as the solution of the following Lyapunov equation:

$$\mathbf{A}\mathbf{C} + \mathbf{C}\mathbf{A}^T = -\mathbf{B}\mathbf{B}^T \,. \tag{8}$$

The co-variance matrix is symmetrical and positive and it can be interpreted as a linear operator that, if applied to a vector of random variables, maps the linear combination of these random variables. This property allows to state that the distribution of the states $\boldsymbol{x}$ can be obtained (for a linear system) directly from the distribution of $\boldsymbol{\eta}$, as follows:

$$\boldsymbol{x} = \mathbf{C}_{x\eta}\mathbf{C}_{\eta\eta}^{-1}\,\boldsymbol{\eta} \,, \tag{9}$$

where we have clustered matrix $\mathbf{C}$ as:

$$\mathbf{C} = \begin{bmatrix} \mathbf{C}_{xx} & \mathbf{C}_{x\eta} \\ \mathbf{C}_{x\eta}^T & \mathbf{C}_{\eta\eta} \end{bmatrix}, \tag{10}$$

where $\mathbf{C}_{xx}$ and $\mathbf{C}_{\eta\eta}$ are the co-variance matrices of $\boldsymbol{x}$ and $\boldsymbol{\eta}$, respectively, and $\mathbf{C}_{x\eta}$ represents the co-variance matrix between deterministic $\boldsymbol{x}$ and stochastic $\boldsymbol{\eta}$ state variables.

In conclusion, for a linear system, $\boldsymbol{x}$ are normally distributed if $\boldsymbol{\eta}$ are normally distributed. And, from (6), one obtains that also $\boldsymbol{y}$ are normally distributed. However, the power system model (1)-(3) is not linear. Thus, it has to be expected that nonlinearity *deforms* the distribution of states and algebraic variables. If the nonlinearity is not symmetrical, it has also to be expected that the distribution of (at least some) variables is skewed. The following two sections demonstrate this statement through two relevant cases, which are also further illustrated in the case study.

B. Asymmetry due to Network Losses

Let us consider a simple one-machine one-load power system as shown in Fig. 1. Let us also assume that the system is at an equilibrium point. The power generated by the machine compensates both the load consumption and the losses in the transmission system:

$$p_G = p_L + p_{\text{loss}}\,, \tag{11}$$

where losses are proportional to the square of the current. Assuming negligible the variations of the voltage, we can write:

$$p_G \approx p_L + \frac{r}{v^2}\, p_L^2\,, \tag{12}$$

where r is resistance of the line and the internal losses of the generator and v is the voltage, which, for simplicity of illustration, we assume constant. Moreover, we assume that initially the frequency of the system is equal to the synchronous reference, namely, $\omega = 1$ pu.

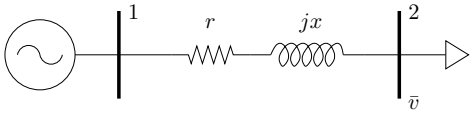

Fig. 1: One-machine one-load system.

Starting from the initial balance in (12), consider a variation of the load consumption Δp_L:

$$\begin{aligned} p_G + \Delta p_G &= p_L + \Delta p_L + \frac{r}{v^2}\,(p_L + \Delta p_L)^2\,, \\ &= p_L + \frac{r}{v^2}\, p_L^2 + 2\frac{r}{v^2}\, p_L \Delta p_L + \frac{r}{v^2}\, \Delta p_L^2\,, \end{aligned} \tag{13}$$

where Δp_G is the active power variation of the generator due to the turbine governor. Assuming that Δp_G is a function of the droop-control of the turbine governor of the machine, in steady-state, one has:

$$\Delta p_G = -\frac{1}{R}\,\Delta\omega\,, \tag{14}$$

where R is the droop coefficient of the turbine governor. Merging (12) and (14) in (13), we obtain:

$$\begin{aligned} \Delta\omega &= -\left(2\frac{R\,r}{v^2}\, p_L\right)\,\Delta p_L - \left(\frac{R\,r}{v^2}\right)\,\Delta p_L^2\,, \\ &= -K_1\,\Delta p_L - K_2\,\Delta p_L^2\,, \end{aligned} \tag{15}$$

which shows that the effect of losses, i.e., the quadratic term, on the frequency deviation $\Delta\omega$ is always positive and thus has an asymmetrical effect on the steady-state value of the frequency. This effect, in turn, impacts the probability distribution of the frequency which is skewed towards the side with $\Delta\omega > 0$ pu, as the effect of losses mitigates negative variations of the load power consumption.

C. Asymmetry due to Wind Frequency Control

The mechanical power p_w extracted from the wind is a nonlinear function of the wind speed v_w, the rotor speed ω_m and the pitch angle θ_p. The mechanical power p_w of the wind turbine can be approximated as:

$$p_w = \frac{\rho}{2} A_r c_p(\lambda, \theta_p)\, v_w^3\,, \tag{16}$$

where v_w is the wind speed; θ_p and λ are the blade pitch angle and speed tip ratio, respectively; A_r is the area of the turbine disk; ρ is the air density. The turbine efficiency function $c_p(\lambda, \theta_p)$ can be approximated as follows [15]:

$$c_p = 0.22\left(\frac{116}{\lambda_i} - 0.4\,\theta_p - 5\right)e^{-\frac{12.5}{\lambda_i}}\,, \tag{17}$$

with

$$\frac{1}{\lambda_i} = \frac{1}{\lambda + 0.08\,\theta_p} - \frac{0.035}{\theta_p^3 + 1}\,, \tag{18}$$

where numerical coefficients are determined empirically. There exist several other alternative empirical expressions for c_p, e.g., [16]. In conventional wind turbines, where the main goal of the generator is to maximize the power extracted from the wind, $\theta_p = 0$ in normal operating conditions and $\theta_p \neq 0$ is utilized exclusively to limit the power of the wind turbine at high wind speeds.

A way to regulate the frequency through wind turbines, equivalent to a power reserve, is to introduce an offset of the pitch angle in normal operating conditions [17]. Then the frequency can be regulated through a droop control:

$$\dot{\theta}_p = \frac{1}{R}\Delta\omega - \theta_p\,. \tag{19}$$

Considering again the load variation Δp_L and assuming for simplicity constant wind speed and thus constant speed tip ratio, and that the power injected into by the wind turbine coincides with the mechanical power p_w, that is, neglecting losses and considering an ideal converter control, in steady state, one has:

$$\Delta\theta_p = -\frac{1}{R}\Delta\omega\,, \tag{20}$$

and hence:

$$\begin{aligned} \Delta p_G &= c_1\,\Delta\theta_p + c_2\,\Delta\theta_p^2 + O(\Delta\theta_p^3)\,, \\ &= -\frac{c_1}{R}\,\Delta\omega + \frac{c_2}{R^2}\,\Delta\omega^2 + O(\Delta\omega^3)\,, \end{aligned} \tag{21}$$

where the coefficient c_1 and c_2 are obtained from the Taylor series expansion of c_p centered at the initial operating point and $O(\Delta\omega^3)$ is the residual terms of order higher than 2. Neglecting high-order terms, (15) obtained in the previous section can be rewritten as follows:

$$c_1\,\Delta\omega - \frac{c_2}{R}\,\Delta\omega^2 = -K_1\,\Delta p_L - K_2\,\Delta p_L^2\,, \tag{22}$$

which can be solved for $\Delta\omega$ and is, as expected, a nonlinear expression linking $\Delta\omega$ and Δp_L. Note that the $c_1 \approx c_2$, and hence $c_1 \ll c_2/R$ as the droop coefficient R is of the order of 10^{-2}. Then, (22) can be simplified as:

$$\Delta\omega^2 \approx \frac{R\,K_1}{c_2}\,\Delta p_L + \frac{R\,K_2}{c_2}\,\Delta p_L^2\,. \tag{23}$$

The examples presented in the case study show that the nonlinearity due to wind frequency regulation obtained using pitch angle control is "stronger" than that due to system losses and thus leads to higher asymmetry.

D. Asymmetry due to Regulator Hard Limits

Another important source of asymmetry in any controller are the hard limits. If a controller operates close to one of its limits, in fact, every time that the limit is binding the effect the regulator becomes inactive, thus, leading to a substantially different behavior of the controlled system. This effect is particularly common in wind generation (with or without primary frequency control) and has been observed specifically in the Irish system when tight deadband are enforced in the primary frequency control of wind turbines. This aspect is further discussed in Sections IV-A and in the case study.

E. Compensation of Asymmetry through Control

In this section, we propose a nonlinear deadband function to reduce asymmetry which uses the frequency deviation $\Delta\omega$ as an input signal, as follows:

$$u(\Delta\omega) = (1-\gamma\Delta\omega)^{\alpha}\Delta\omega^{\beta}\,, \tag{24}$$

where γ and α are adjustable parameters. Substituting the expression (24) into (14) one obtains:

$$\Delta p_G = -\frac{1}{R}u(\Delta\omega)\,, \tag{25}$$

and, hence, (15) becomes:

$$(1-\gamma\Delta\omega)^{\alpha}\Delta\omega^{\beta} = -K_1\Delta p_L - K_2\Delta p_L^2\,. \tag{26}$$

If one chooses $\alpha = \beta = 1$ and $\gamma = K_2$, then:

$$\Delta\omega = -K_1\Delta p_L\,, \tag{27}$$

which leads to a linear (symmetric) controller where nonlinearity due to losses is fully compensated.

Similarly, if in (20) one implements that proposed controllers, and sets $\alpha = \beta = 0.5$ and $\gamma = R\,K_2/c_2$, (23) can be rewritten as:

$$\Delta\omega \approx -\frac{R\,K_1}{c_2}\,\Delta p_L\,. \tag{28}$$

which, again, is a linear expression and makes the pitch-angle frequency control symmetric.

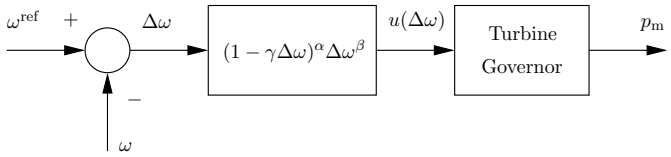

Fig. 2: Proposed nonlinear compensation for turbine governors of synchronous machines.

As the expressions (15) and (23) are obtained through approximated models where higher order terms are neglected, and as the coefficient K_2 depends on the operating point, it is not possible, in general, to obtain a full compensation of the losses. Based on several tests, for example, we have determined empirically that $\alpha = 0.5$ and $\beta = \gamma = 1$ work well in the simulated-based scenario considered in the case study for turbine governors of conventional power plants.

III. Metrics

To measure asymmetry, we propose to calculate the left and right-hand side standard deviations of the frequency PDs, namely "negative" (σ_{f-}) for when the frequency is below the nominal (f_n) (sample size N_-) and "positive" (σ_{f+}) when frequency is above f_n (sample size N_+). Then, we calculate the frequency standard deviation σ_f using a weighted-average method of the two standard deviations (σ_{f-}, σ_{f+}). Next, the asymmetry $\Delta\sigma_f$ is defined as the difference between σ_{f-} and σ_{f+}. These equations are shown below:

$$\sigma_{f-} = \sqrt{\frac{1}{N_-}\sum_{i=1}^{N_-}(f_i - f_n)^2}\,,\ \{f_i : f_i < f_n\}\,, \tag{29}$$

$$\sigma_{f+} = \sqrt{\frac{1}{N_+}\sum_{i=1}^{N_+}(f_i - f_n)^2}\,,\ \{f_i : f_i > f_n\}\,, \tag{30}$$

$$\sigma_f = \sqrt{\frac{1}{N}\sum_{i=1}^{N}(f_i - f_n)^2} \approx \sqrt{\frac{N_+\sigma_{f+}^2 + N_-\sigma_{f-}^2}{N_+ + N_-}}\,, \tag{31}$$

$$\Delta\sigma_f = |\sigma_{f-} - \sigma_{f+}|\,. \tag{32}$$

Note that the expressions in (31) are substantially equal as, in practice, very few measurements are exactly equal to f_n.

As there are other existing asymmetry-based metrics used in the literature such as the skewness parameter, β_f, we calculate and compare it, where relevant, with $\Delta\sigma_f$. The skewness β_f is defined as follows [11]:

$$\beta_f = \frac{1}{N}\sum_{i=1}^{N}\left(\frac{f_i - \mu_f}{\sigma_f}\right)^3\,, \tag{33}$$

where μ_f is the mean of system frequency. Note that if β_f equals to zero the distribution is Gaussian (symmetric). In contrast, a non-zero skewness (β_f) implies a distribution that is not symmetric.

Another key metric of frequency quality used by TSOs is the so-called 100 mHz criteria which measures the minutes frequency spends outside the $\pm$100 mHz range (i.e., keep frequency within this range for more than 98% of the time) [18]. We calculate these minutes in relevant scenarios discussed in Section V.

IV. Asymmetry in Real-World Power Systems

This section provides evidence of FPD asymmetry based on measurements obtained from EirGrid, TSO in Ireland, and from AEMO, the Australian energy market operator.

A. Real-World Data from the Irish Grid

We first show the appearance of asymmetry in a real-world system with high shares of wind generation, namely the Irish power system [19]. With this aim, we select three relevant hours with the following details:

- Scenario 1: Deadband of wind farms is $\pm$200 mHz and thus APC (i.e., a PFC with a tight $\pm$ 15 mHz deadband) is turned Off.
- Scenario 2: Deadband of wind farms is reduced to $\pm$15 mHz and thus APC is turned On.
- Scenario 3: Represents conventional power systems with near-zero wind generation and APC Off (i.e., $\pm$200 mHz deadband).

Further details on each scenario can be found in Table I. Note that currently in the Irish power system APC is normally disabled. The APC is enabled in special circumstances, e.g., during periods of high export or if there are severe frequency oscillations in the system [12].

In the remainder of this section, we consider three measurement data sets obtained from the TSOs historical information system (coming from SCADA and stored in 1 second resolution) and calculate σ_f, $\Delta\sigma_f$ and minutes outside the $\pm$100 mHz range. It is worth mentioning that AGC is not utilized in the Irish power system. Table V summarizes these scenarios. Further information on the operating conditions for each scenario can be found online in [20].

Scenarios 1 and 2. These two scenarios correspond to the 27 of January 2024, namely 6 consecutive hours, 3 when APC was Off and 3 when APC was turned On. The Irish power system experienced high wind generation around 3.5 GW. Note that the peak demand of the Irish system is just above 7 GW and valley demand is less than 2.5 GW. In these 6 hours, the system non-synchronous penetration was around 72% on average and system conditions remained almost the same, at least, in terms of wind generation, number of conventional units online (i.e., 7) and demand.

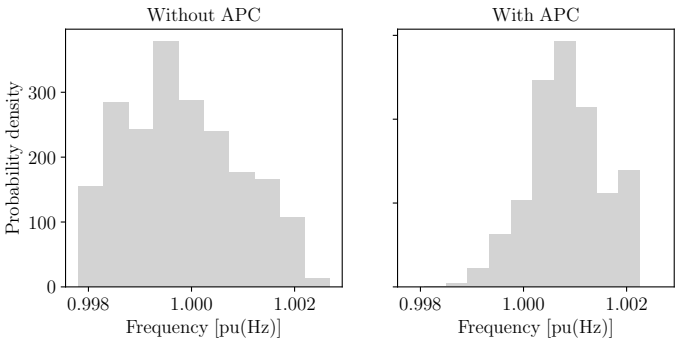

Fig. 3: FPD of the Irish power system with and without APC.

Figure 3 depicts the FPDs for both scenarios, namely with and without APC. APC Off leads to a normal distribution and symmetric behaviour of the FPD. It can be inferred from Table II, in fact, that the asymmetry for the 3 hours when APC was Off (Scenario 1) is very small and similar to Scenario 4 in the IEEE 9-bus system (see Table VI below). The minutes outside the $\pm$100 mHz range are also small. It is worth pointing out that whenever the frequency drifts away from the $\pm$100 mHz range, the operators take manual actions (e.g., conventional generation redispatch) to bring back frequency within the range.

On the other hand, Fig. 3 shows that when APC is enabled (Scenario 2) to reduce the frequency oscillations (all 6 APC groups [12]) it seriously increases the asymmetry of the FPD (this scenario is equivalent to Scenario 10 in Table VI below). Specifically, it can be seen from the results in Table II that while the average standard deviation (σ_f) is more or less the same with Scenario 1, the asymmetry $\Delta\sigma_f$ has increased dramatically. In fact, the asymmetry is very similar to that considered in Scenario 10 for the IEEE 9-bus system. The asymmetry can also be observed in the minutes outside the $\pm$100 mHz range. Note that we tested other real-world scenarios when APC was Off and On and obtained similar results. Note also that while wind turbines may operate based on nonsymmetric droop characteristic (i.e., which could then be a potential source of asymmetry) [21], that is not the case in the Irish power grid (symmetric droop is used instead).

Scenario 3. This scenario refers to 20th April 2024 and represents a conventional power system with near-zero wind generation as wind levels in the Irish power system during this particular period were around 50 MW. This scenario thus allows for an interesting comparison with respect to the Scenarios 1 and 2 with high wind shares (i.e., 3.5 GW).

Results suggest that σ_f, $\Delta\sigma_f$ and minutes outside the $\pm$100 mHz range are reduced compared to Scenario 2. However, compared to Scenario 1, the asymmetry ($\Delta\sigma_f$) is increased significantly. This can be explained by the fact that being a near-zero wind generation condition means that the conventional generators online and interconnectors should operate closer to their maximum limits [20].

B. Real-World Data from the Australian Grid

As anticipated in the introduction, the asymmetry in the Australian (mainland) power system has recently raised concerns. We select three years with different deadband implementations namely 2010 ($\pm$30-50 mHz), 2019 ($>\pm$150 mHz) and 2023 ($\pm$15 mHz) to compare the asymmetry evolution (see Table III). Specifically, it is worth pointing out that prior to 2015 the deadband settings in mainland were generally set within a range of $\pm$ 30 mHz to $\pm$ 50 mHz [1]. Whereas in 2016 the decisions of the Australian Energy Regulator and Market Commission not to enforce generator participants a specific deadband made the latter changing (widening) their deadbands (e.g., $\pm$ 150 mHz) effectively resulting in no PFC in the standard frequency range $\pm$ 150 mHz. Finally, in 2020 the mandatory PFC rule with $\pm$ 15 mHz deadband was enforced motivated by a deterioration of frequency quality.

Table IV presents all the relevant results, while Fig. 4 depicts the FPD for years 2023 and 2019 (frequency recordings are made publicly available by AEMO). It is interesting to observe that while σ_f and minutes outside $\pm$ 150 mHz

TABLE I: Scenario description for the Irish power system.

Scenario	Wind Generation	APC	fdb_{wind} (mHz)	fdb_{conv} (mHz)	AGC conv/wind	Wind Ramps	Load Noise	Wind Noise	Losses	Saturation	$\text{fdb}_{\text{model}}$
1	Yes	Off	$\pm$ 200	$\pm$ 15	No	Yes	Yes	Yes	Normal	No	–
2	Yes	On	$\pm$ 15	$\pm$ 15	No	Yes	Yes	Yes	Normal	No	–
3	Yes	Off	$\pm$ 200	$\pm$ 15	No	Yes	Yes	Yes	Normal	No	–

TABLE II: Summary of results for the Irish power system.

Scenario	σ_f (Hz)	σ_{f-} (Hz)	σ_{f+} (Hz)	$\Delta\sigma_f$ (Hz)	Minutes Outside $\pm$100mHz	Minutes Outside $+$100mHz	Minutes Outside $-$100mHz	P_{loss} (pu)	Q_{loss} (pu)
1	0.0558	0.0557	0.0560	0.0003	6.6	3.8	2.8	–	–
2	0.0547	0.0259	0.0575	0.0316	7	7	0	–	–
3	0.030	0.0359	0.0152	0.0207	0	0	0	–	–

TABLE III: Scenario description for the Australian (mainland) power system for years 2010, 2019 and 2023.

Year	Wind Generation	APC	fdb_{wind} (mHz)	fdb_{conv} (mHz)	AGC conv/wind	Wind Ramps	Wind Noise	Losses	Saturation
2010	Yes	Off	$\pm$ 30 – 50	$\pm$ 30 – 50	Yes	Yes	Yes	–	–
2019	Yes	Off	$> \pm$ 150	$> \pm$ 150	Yes	Yes	Yes	–	–
2023	Yes	On	$\pm$ 15	$\pm$ 15	Yes	Yes	Yes	–	–

TABLE IV: Summary of asymmetry results for the Australian (mainland) power system for years 2010, 2019 and 2023.

Year	σ_f (Hz)	σ_{f-} (Hz)	σ_{f+} (Hz)	$\Delta\sigma_f$ (Hz)	Minutes Outside $\pm$150mHz	Minutes Outside $+$150mHz	Minutes Outside $-$150mHz	β_f (Hz)
2010	0.0286	0.0294	0.0282	0.0011	137.13	4.4	132.73	-0.18
2019	0.0635	0.0647	0.0643	0.00032	4059	841	3218	-0.047
2023	0.0256	0.0271	0.0244	0.00267	3.4	0.133	3.266	-0.221

have dramatically decreased in 2023 compared to 2010 and 2019, that is not the case for the asymmetry. Specifically, the asymmetry for 2023 equals $\Delta\sigma_f$= 0.00267 Hz compared to just 0.00032 Hz and 0.0011 Hz in 2019 and 2010, respectively. As mentioned above, the main change after 2020 is the introduction of mandatory PFC provision with $\pm$ 15 mHz deadband (i.e., APC-type). The asymmetry in each case can also be observed in the minutes outside $\pm$150 mHz range. In particular, it is worth mentioning that there is no surprise in the degradation of frequency performance in 2019 (i.e, significant increase in the minutes outside $\pm$150 mHz) given the wider deadband implementation by generators. These results from the Australian power system further support the theoretical insights and observations in the Irish grid (and also the conclusions of the case study below) that narrow frequency deadbands from RESs (e.g., wind generation) lead to substantially increase the asymmetry of the FPD.

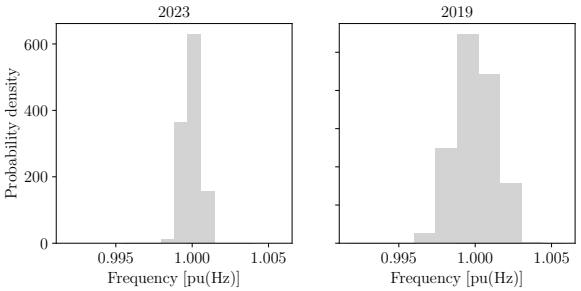

Fig. 4: FPD of the Australian (mainland) power system for 2023 and 2019 years.

Finally, we calculate the skewness parameter β_f as another metric of asymmetry and to allow comparing it with $\Delta\sigma_f$. Table IV suggests that while β_f is at least two orders of magnitude higher than $\Delta\sigma_f$, it is consistent with $\Delta\sigma_f$ in terms of it being higher for year 2023 (-0.221 Hz) compared to years 2019 (-0.047 Hz) and 2010 (-0.18 Hz), respectively. It is also worth pointing out that all β_f values take a negative sign indicating a leftward skew with a longer tail for negative values of the frequency distribution. This is also consistent with the results of the standard deviation-based metrics, that is, σ_{f-} being higher than σ_{f+} in all cases.

V. Case Study

To analyse the statistical properties of the frequency we run long-term time-domain simulations, namely 48h, based on the SDAE model (1)-(3) and all simulations are solved with software tool Dome [22]. The results shown in this section are obtained using the IEEE 9-bus system, adapted for the various considered scenarios for a comprehensive evaluation of the different sources of asymmetry. A short description of each scenario is provided below. Table V provides relevant information on setup and controllers and Table VI shows simulation results for each scenario.

- *Scenario 4*: Conventional power systems without wind generation. Synchronous generators have a $\pm$15 mHz governor deadband and AGC.
- *Scenario 5*: Same as Scenario 4 but with increase of network losses.
- *Scenario 6*: Same as Scenario 5 but with inclusion of the proposed nonlinear compensation in the PFC of synchronous generators.
- *Scenario 7*: Studies the effect of saturation on the FPD.
- *Scenario 8*: Power system with wind generation providing PFC with $\pm$200 mHz deadband (APC Off).
- *Scenario 9*: Same as Scenario 8 but with $\pm$15 mHz deadband (APC On).
- *Scenario 10*: Same as Scenario 9 and with wind ramps modelled based on realistic data from the Irish system.
- *Scenario 11*: Same as Scenario 10 but with AGC installed (only conventional power plants).

TABLE V: Scenario description for the IEEE 9-bus system.

Scenario	Wind Generation	APC	fdb_{wind} (mHz)	fdb_{conv} (mHz)	AGC conv./wind	Wind Ramps	Wind Noise	Losses	Saturation	Compensation Eq. (24)
4	–	–	–	± 15	conv.	–	–	Normal	–	–
5	–	–	–	± 15	conv.	–	–	High	–	–
6	–	–	–	± 15	conv.	–	–	High	–	Yes
7	–	–	–	–	–	–	–	Normal	Yes	–
8	Yes	Off	± 200	–	–	–	Gaussian	Normal	–	–
9	Yes	On	± 15	–	–	–	Gaussian	Normal	–	–
10	Yes	On	± 15	–	–	Yes	Gaussian	Normal	–	–
11	Yes	On	± 15	–	conv.	Yes	Gaussian	Normal	–	–
12	Yes	Off	± 200	–	conv. & wind	Yes	Gaussian	Normal	–	–
13	Yes	On	± 15	–	conv. & wind	Yes	Gaussian	Normal	–	–
14	Yes	On	± 15	–	conv. & wind	Yes	Gaussian	Normal	–	Yes
15	Yes	On	± 15	–	conv. & wind	Yes	Weibull	Normal	–	–

TABLE VI: Summary of simulation results for the IEEE 9-bus system.

Scenario	σ_f (Hz)	σ_{f-} (Hz)	σ_{f+} (Hz)	$\Delta\sigma_f$ (Hz)	Minutes Outside ± 100mHz	Minutes Outside $+100$mHz	Minutes Outside -100mHz	P_{loss} (pu)	Q_{loss} (pu)
4	0.0107	0.0108	0.0107	0.0001	0	0	0	0.0409	-0.9452
5	0.0314	0.0330	0.0294	0.0036	5.28	1.27	4.00	0.5097	-0.6151
6	0.0350	0.0349	0.0350	0.00007	10.8	6.44	4.35	0.5097	-0.6151
7	0.0236	0.0245	0.0227	0.0018	0.2233	0.0183	0.205	0.0409	-0.9452
8	0.0602	0.0606	0.0598	0.0008	280.49	136.38	144.10	–	–
9	0.0803	0.0841	0.0762	0.0079	611.41	287.69	323.71	–	–
10	0.1085	0.1254	0.0868	0.0386	1073.61	456.67	616.94	–	–
11	0.0794	0.0845	0.0745	0.01	575.79	267.32	308.47	–	–
12	0.0635	0.0629	0.0641	0.0012	314.91	152.70	162.20	–	–
13	0.0591	0.0630	0.0555	0.0074	–	–	–	–	–
14	0.0649	0.0660	0.0638	0.0021	–	–	–	–	–
15	0.1044	0.110	0.0994	0.0105	–	–	–	–	–

- *Scenario 12*: Wind farms provide AGC functionality with APC Off.
- *Scenario 13*: Wind farms provide AGC functionality with APC On.
- *Scenario 14*: Same as Scenario 13; APC includes the proposed nonlinear compensation to reduce asymmetry.
- *Scenario 15*: Same as Scenario 13 with Weibull-distributed, i.e., asymmetric, wind speed fluctuations.

For all scenarios, load consumption includes Gaussian noise modelled as mean-reverted Ornstein-Uhlenbeck processes and stochastic jumps as described in [13] and [23], respectively.

A. Power Systems with Conventional Generation

In this first section, we focus on the asymmetry that exists in conventional power systems. Two potential sources of asymmetry are considered, namely, losses and control limiters.

Scenario 4: This scenario represents conventional power systems with synchronous machines providing both PFC and AGC [24]. The main source of volatility in this scenario is noise in loads modelled as a stochastic process that incorporates both continuous and event-driven (jumps) dynamics. This is based on real-world behaviour of loads in the Irish power system [23]. Figure 5(a) depicts the center of inertia FPD. As expected, the FPD shows a normal/Gaussian distribution and symmetric behavior. These results are confirmed in Table VI, which shows that the asymmetry calculated using (32) is small ($\Delta\sigma_f = 0.0001$ Hz) and the minutes outside the ± 100 mHz range are zero.

The main goal of the AGC is to eliminate the frequency error, that is, difference between the reference frequency and the measured frequency at a pilot bus of the system, through an integral controller as shown in Fig. 6 [24]. As it shrinks the frequency distribution (see., e.g., [8]), the AGC is beneficial to reduce the effects of the asymmetries present in the system.

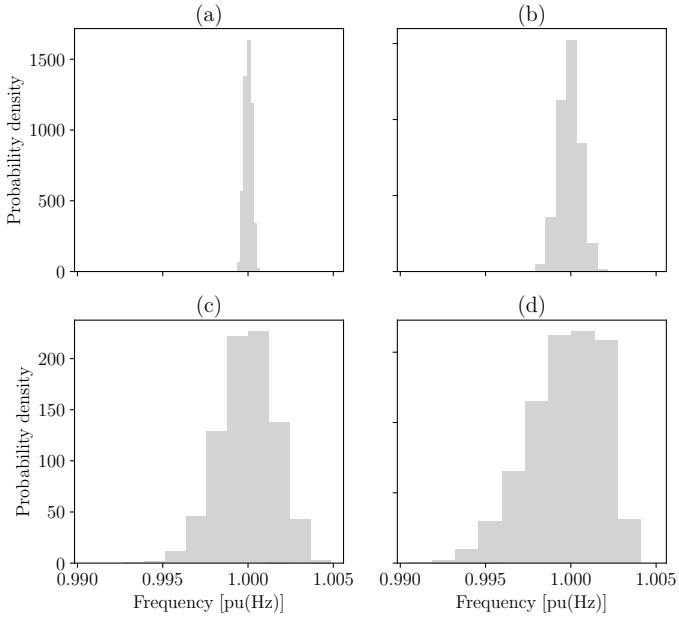

Fig. 5: PD of: (a) Scenario 4, conventional power systems; (b) Scenario 5, high losses; (c) Scenario 9, APC On and no wind ramps; and (d) Scenario 10, APC On and wind ramps.

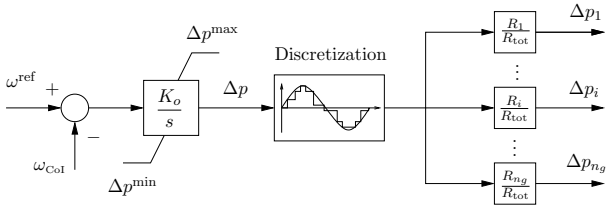

Fig. 6: AGC control diagram. The discretized output signals Δp_i are sent to the PFC of synchronous generators and wind power plants.

Scenario 5: Here we focus on the impact that the increase of system losses have on the FPD. For illustration purposes, we increase the resistance of transmission lines by ten times (this

can represent distribution systems). Figure 5(b) shows that losses have a significant impact on the FPD and its asymmetry. Moreover, Table VI shows that, compared to Scenario 4, $\Delta\sigma_f$ has increased from $\Delta\sigma_f = 0.0001$ Hz to $\Delta\sigma_f = 0.0036$ Hz. Consequently, the standard deviation and the 100 mHz criteria have also increased.

Scenario 6: This scenario explores the effectiveness of the proposed nonlinear compensation model presented in Section II-E in removing/reducing the asymmetry. With this aim, we select the case with high losses (Scenario 5) and set the values of γ and α to 1 and 0.5, respectively (of course, other values might be used). Results from Table VI indicate that the asymmetry is reduced significantly (from $\Delta\sigma_f$ = 0.0036 Hz to $\Delta\sigma_f$ = 0.00007 Hz). Therefore, this compensation can be considered as a viable option for TSOs operating grids with high asymmetry of the frequency distribution.

Scenario 7: In this scenario we simulate the effect of saturation/limits (highly loaded systems). Specifically, we assume that the maximum power of synchronous generator 1 and 2 are reduced by approximately 40% and 50%, respectively. As expected, the results of Table VI indicate an increase in the asymmetry in the FPD compared to, for example, Scenario 4, but lower compared to Scenario 5 that considers high network losses.

B. Power Systems with Non-Synchronous Generation

This section discusses the effect of wind generation and its control under different scenarios. In particular, the aim is to see whether the introduction of wind and its frequency control/regulation capability in the power system affects the asymmetry of the FPD. With this aim, we consider again the WSCC 9-bus system and replace the synchronous generator 3 with a wind power plant modelled as a double-fed induction generator [25]. We assume that the wind power plant provides frequency regulation through droop-based PFC with tight deadband namely $\pm$15 mHz (same used by the governors of conventional generators), as is the case in the Irish power system [18]. This is also known as wind/solar farm APC [12]. To be able to provide up and down regulation, we assume wind is operating 20% below its maximum power point tracking (i.e., curtailed). The description of Scenarios 8-15 is provided in Table V.

Scenario 8: We assume that wind farms provide frequency support only to respond to contingency events (deadband of $\pm$200 mHz). Note that since in practice frequency rarely goes outside the $\pm$200 mHz range during a day (except in very small island power systems and/or microgrids), it can be said that wind farms provide regular wind generation. We also model noise from wind and loads as Gaussian noise, i.e., $\boldsymbol{b}$ is a constant vector, but no jumps, i.e., $\boldsymbol{c} = \mathbf{0}$, in (3). Results in Table VI indicate that the inclusion of wind farms increase σ_f, the asymmetry ($\Delta\sigma_f = 0.0008$ Hz) and minutes outside the 100 mHz range compared to conventional power systems without wind (e.g., Scenario 4).

Scenario 9: This scenario considers the effect of wind farms providing APC functionality through the $\pm$15 mHz deadband (i.e., this means they are continuously providing dynamic primary frequency regulation since frequency moves outside the $\pm$15 mHz deadband on a regular basis during a day). Noise is same as in Scenario 8. Figure 5(c) and Table VI show relevant results. Surprisingly, the APC leads to increase σ_f and the asymmetry of the FPD (from $\Delta\sigma_f = 0.0008$ Hz to $\Delta\sigma_f = 0.0079$ Hz). These results are a consequence of the nonlinearity of the wind turbine, i.e., the cubic relationship between wind speed and turbine torque.

Scenario 10: In addition to wind farms providing APC functionality, here we also consider wind ramps modelled based on realistic profile from the Irish power system. Ramps are obtained through stochastic jumps in (3) as described in [23]. Results are shown in Table VI. The standard deviation ($\sigma_f = 0.1085$ Hz), asymmetry ($\Delta\sigma_f = 0.0386$ Hz) and minutes outside the $\pm$100 mHz range (1073.61) have dramatically increased compared to the previous scenario. To illustrate this, we plot in Figure 5(d) the FPD. It is striking to see that the behavior of the FPD is quite asymmetric.

Scenario 11: This is the same scenario as Scenario 10 but now with AGC (only conventional generators). Looking at the results in Table VI we can see now that AGC significantly reduces σ_f (from 0.1085 Hz to 0.0794 Hz), the asymmetry (from $\Delta\sigma_f = 0.0386$ Hz to $\Delta\sigma_f = 0.01$ Hz) and minutes outside the $\pm$100 mHz range (from 1073.61 to 575.79). Thus, the AGC appears as a viable solution to reduce the frequency asymmetry in power systems and help keep frequency quality within limits.

Scenario 12: The asymmetry of the FPD and dynamic behaviour of the system can be improved if wind is also providing AGC functionality (but with APC Off). This is shown in Table VI where we can see that σ_f, $\Delta\sigma_f$ and minutes outside the $\pm$100 mHz range are improved significantly with the inclusion of wind farms in AGC.

Scenario 13: This is the same as Scenario 12 but now we reduce the deadband of wind farms to $\pm$15 mHz (i.e., turn On APC) to see its impact on assymetry. Interestingly, making wind farms adjust their MW output much more dynamically to control frequency under normal, pre-contingency, conditions leads to an increase of $\Delta\sigma_f$ namely from 0.0012 Hz (Scenario 12) to 0.0074 Hz (this Scenario). These results support the observations in the Irish and Australian power grids where higher asymmetry is observed when RESs provide APC-type frequency regulation.

Scenario 14: In this scenario, we check the effectiveness of the nonlinear deadband implementation in wind farms in reducing the asymmetry. With this aim, we set the values of Γ and B to 2 and 0.2, respectively. Compared to the previous scenario, it can be seen that $\Delta\sigma_f$ is reduced by more than three times namely from 0.0074 Hz to 0.0021 Hz. Therefore, such a deadband implementation might be considered as a potential solution by TSOs.

Scenario 15: Finally, it is relevant to study the effect of different wind speed noise distributions on the frequency asymmetry, namely, Gaussian (symmetric) and Weibull distribution (asymmetric). The interested reader can find the details of the model of the wind speed based on Weibull distribution in [26]. Table VI shows that the Weibull noise leads to a higher asymmetry ($\Delta\sigma_f$ = 0.0105 Hz) compared to the Gaussian

noise ($\Delta\sigma_f$ = 0.0074 Hz), as expected. We note however that, short-term wind speed fluctuations are better represented as Gaussian noise around an average value [27]. Such an average, calculated across periods of, say, an hour, is distributed as a Weibull or other non-symmetrical distributions. The main source of asymmetry (nonlinearity) due to wind generation is thus not the wind speed but its turbine and its frequency control.

VI. Conclusions

This paper presents a comprehensive analysis of various sources of asymmetry of FPD in power systems. With this aim, the paper first provides analytical insights on the causes of asymmetrical distribution of the frequency. Next, the paper proposes a nonlinear compensation suitable for both turbine governors of conventional synchronous machines as well as for the frequency control of variable-speed wind generators. We also propose a new metric based on the difference between the standard deviations of the FPD to evaluate the system asymmetry. This metric allows consistently comparing asymmetry in different power systems without knowledge of specific parameters and/or system conditions.

Real-world data from the Irish and Australian power systems and a case study based on the IEEE 9-bus system serve to show that RESs (e.g., wind generation) are significant sources of asymmetry, in particular, when providing dynamic frequency regulation through narrow deadband such as $\pm$ 15 mHz. As mentioned in Section I, this is already a serious issue being discussed currently in Australia. The Irish TSOs also recognize the potential appearance of new phenomena as part of the need to have $\pm$ 15 mHz minimum deadband capability from more reserve service providers [28]. It is also shown that AGC is a viable solution to reduce FDP asymmetry.

Future work will focus on evaluating FDP asymmetry of other real-world power systems and explore alternative control-based options to minimize this asymmetry.

References

[1] CS Energy, "Submission: Draft determination - review of the frequency operating standard," 2023. [Online]. Available: https://www.aemc.gov.au/

[2] AEMO, "Primary frequency response requirements," 2023. [Online]. Available: https://aemo.com.au/

[3] M. Martínez-Barbeito, D. Gomila, and P. Colet, "Dynamical model for power grid frequency fluctuations: Application to islands with high penetration of wind generation," *IEEE Trans. on Sustainable Energy*, vol. 14, no. 3, pp. 1436–1445, 2023.

[4] D. Kraljic, "Towards realistic statistical models of the grid frequency," *IEEE Trans. on Power Systems*, vol. 38, no. 1, pp. 256–266, 2023.

[5] D. del Giudice, A. Brambilla, S. Grillo, and F. Bizzarri, "Effects of inertia, load damping and dead-bands on frequency histograms and frequency control of power systems," *Int. J. of Electrical Power & Energy Systems*, vol. 129, p. 106842, 2021.

[6] L. R. Gorjão, M. Anvari, H. Kantz, C. Beck, D. Witthaut, M. Timme, and B. Schäfer, "Data-driven model of the power-grid frequency dynamics," *IEEE Access*, vol. 8, pp. 43 082–43 097, 2020.

[7] P. Vorobev *et al.*, "Deadbands, droop, and inertia impact on power system frequency distribution," *IEEE Trans. on Power Systems*, vol. 34, no. 4, pp. 3098–3108, 2019.

[8] F. M. Mele, Á. Ortega, R. Zárate-Miñano, and F. Milano, "Impact of variability, uncertainty and frequency regulation on power system frequency distribution," in *Power Systems Computation Conference (PSCC)*, 2016, pp. 1–8.

[9] F. Milano, F. Dörfler, G. Hug, D. J. Hill, and G. Verbič, "Foundations and challenges of low-inertia systems (invited paper)," in *2018 Power Systems Computation Conference (PSCC)*, 2018, pp. 1–25.

[10] X. Wen, M. Anvari, L. R. Gorjao, G. C. Yalcin, V. Hagenmeyer, and B. Schäfer, "Non-standard power grid frequency statistics in Asia, Australia, and Europe," *arXiv preprint arXiv:2308.16842*, 2023.

[11] B. Schäfer *et al.*, "Non-Gaussian power grid frequency fluctuations characterized by Lévy-stable laws and superstatistics," *Nature Energy*, vol. 3, no. 2, pp. 119–126, 2018.

[12] EirGrid & SONI, "Active power control groups," 2020. [Online]. Available: https://www.sem-o.com/

[13] F. Milano and R. Zárate-Miñano, "A systematic method to model power systems as stochastic differential algebraic equations," *IEEE Trans. on Power Systems*, vol. 28, no. 4, pp. 4537–4544, 2013.

[14] H. J. Carmichael, *Statistical methods in quantum optics 1: master equations and Fokker-Planck equations*. Springer Science & Business Media, 2013.

[15] S. Heier, *Grid Integration of Wind Energy Conversion Systems*. Chichester, England: John Wiley & Sons, 1998.

[16] J. Slootweg, S. de Haan, H. Polinder, and W. Kling, "General Model for Representing Variable Speed Wind Turbines in Power System Dynamics Simulations," *IEEE Trans. on Power Systems*, vol. 18, no. 1, pp. 144–151, Feb. 2003.

[17] T. Wang *et al.*, "A new control strategy of DFIG-based wind farms for power system frequency regulation," in *IEEE PES Asia-Pacific Power and Energy Eng. Conf.*, 2015, pp. 1–5.

[18] T. Kërçi, M. Hurtado, M. Gjergji, S. Tweed, E. Kennedy, and F. Milano, "Frequency quality in low-inertia power systems," in *IEEE PES General Meeting*, 2023, pp. 1–5.

[19] M. Hurtado *et al.*, "Analysis of wind energy curtailment in the Ireland and Northern Ireland power systems," in *IEEE PES General Meeting*, 2023, pp. 1–5.

[20] EirGrid, "Real time system information," 2024. [Online]. Available: https://www.eirgrid.ie/grid/real-time-system-information

[21] E. Ela *et al.*, "Active power controls from wind power: Bridging the gaps," National Renewable Energy Lab.(NREL), Golden, CO (United States), Tech. Rep., 2014.

[22] F. Milano, "A Python-based software tool for power system analysis," in *IEEE PES General Meeting*, 2013, pp. 1–5.

[23] F. M. Mele, R. Zárate-Miñano, and F. Milano, "Modeling load stochastic jumps for power systems dynamic analysis," *IEEE Trans. on Power Systems*, vol. 34, no. 6, pp. 5087–5090, 2019.

[24] T. Kërçi, M. A. A. Murad, I. Dassios, and F. Milano, "On the impact of discrete secondary controllers on power system dynamics," *IEEE Trans. on Power Systems*, vol. 36, no. 5, pp. 4400–4409, 2021.

[25] F. Milano, *Power System Modelling and Scripting*. London, UK: Springer, 2010.

[26] R. Zárate-Miñano, M. Anghel, and F. Milano, "Continuous wind speed models based on stochastic differential equations," *Applied Energy*, vol. 104, pp. 42–49, 2013.

[27] G. M. Jónsdóttir and F. Milano, "Data-based continuous wind speed models with arbitrary probability distribution and autocorrelation," *Renewable Energy*, vol. 143, pp. 368–376, 2019.

[28] EirGrid & SONI, "Day-ahead system services auction (DASSA) product review & locational methodology recommendation paper," 2024. [Online]. Available: https://www.eirgrid.ie